








CG7630 is the *Drosophila melanogaster* homolog of the cytochrome c oxidase subunit COX7B

Michele Brischigliaro^{1,*} , Alfredo Cabrera-Orefice² , Mattia Sturlese³, Dei M Elurbe⁴, Elena Frigo¹, Erika Fernandez-Vizarra^{1,5} , Stefano Moro³, Martijn A Huynen⁴ , Susanne Arnold^{2,6} , Carlo Viscomi¹  & Massimo Zeviani^{5,7,**} 

Abstract

The mitochondrial respiratory chain (MRC) is composed of four multiheteromeric enzyme complexes. According to the endosymbiotic origin of mitochondria, eukaryotic MRC derives from ancestral proteobacterial respiratory structures consisting of a minimal set of complexes formed by a few subunits associated with redox prosthetic groups. These enzymes, which are the “core” redox centers of respiration, acquired additional subunits, and increased their complexity throughout evolution. Cytochrome c oxidase (COX), the terminal component of MRC, has a highly interspecific heterogeneous composition. Mammalian COX consists of 14 different polypeptides, of which COX7B is considered the evolutionarily youngest subunit. We applied proteomic, biochemical, and genetic approaches to investigate the COX composition in the invertebrate model *Drosophila melanogaster*. We identified and characterized a novel subunit which is widely different in amino acid sequence, but similar in secondary and tertiary structures to COX7B, and provided evidence that this object is in fact replacing the latter subunit in virtually all protostome invertebrates. These results demonstrate that although individual structures may differ the composition of COX is functionally conserved between vertebrate and invertebrate species.

Keywords cytochrome c oxidase; *D. melanogaster*; COX7B; respiratory chain; mitochondria

Subject Category Metabolism

DOI 10.15252/embr.202254825 | Received 9 February 2022 | Revised 16 May 2022 | Accepted 27 May 2022 | Published online 14 June 2022

EMBO Reports (2022) 23: e54825

Introduction

Cytochrome c oxidase (COX), also known as complex IV (CIV), is the terminal multiheteromeric enzyme of the mitochondrial respiratory chain (MRC). COX, which is part of the heme-copper oxidase superfamily, catalyzes the oxidation of cytochrome c and the reduction of dioxygen to water. The eukaryotic mitochondrial COX is an *aa*₃-type oxidase, sharing similarities with that found in some prokaryotes (Pereira *et al*, 2001; Esposti, 2020). However, the exact molecular evolution of this enzyme is still obscure. Bacterial *aa*₃ oxidases form the minimal catalytically active unit of COX. They are composed of only three polypeptides (commonly named as COX1, COX2, and COX3). COX1 contains two heme A moieties, forming the *aa*₃ center, and a mononuclear copper center (Cu_B), whereas COX2 binds a binuclear copper center (Cu_A). Contrariwise, COX3 contains no prosthetic groups, but it is known to prevent the enzyme's redox-induced irreversible self-damage via a phenomenon named “suicide inactivation” (Bratton *et al*, 1999; Sharma *et al*, 2015). During the evolution of eukaryotes, the genes encoding COX1, COX2, and COX3 were retained in the mitochondrial DNA (mtDNA). Like most MRC complexes, eukaryotic COX expanded throughout evolution, by acquiring a set of so-called “ancillary” or “supernumerary” subunits (Huynen *et al*, 2013). Despite not directly involved in catalysis, the supernumerary subunits participate in the enzyme activity, by conferring structural stability to the core and/or tuning the enzyme kinetics (Čunátová *et al*, 2020). The importance of these subunits is underscored by the observation that, albeit very rare, their pathological mutations lead to COX deficiency and disease phenotypes in humans and animal models (Brischigliaro & Zeviani, 2021). Yeast COX contains nine ancillary subunits (named Cox4-9, Cox12, Cox13, and Cox26; Hartley *et al*, 2019), whereas mammalian COX is composed of 11 subunits around the catalytic core (COX4, COX5A-B, COX6A-C, COX7A-C, COX8, and NDUFA4/

1 Department of Biomedical Sciences, University of Padova, Padova, Italy

2 Radboud Institute for Molecular Life Sciences, Radboud University Medical Center, Nijmegen, The Netherlands

3 Molecular Modeling Section, Department of Pharmaceutical and Pharmacological Sciences, University of Padova, Padova, Italy

4 Centre for Molecular and Biomolecular Informatics, Radboud University Medical Center, Nijmegen, The Netherlands

5 Veneto Institute of Molecular Medicine, Padova, Italy

6 Cologne Excellence Cluster on Cellular Stress Responses in Aging-Associated Diseases (CECAD), University of Cologne, Cologne, Germany

7 Department of Neurosciences, University of Padova, Padova, Italy

*Corresponding author. Tel: +39 049 8278272; E-mail: michele.brischigliaro@unipd.it

**Corresponding author. Tel: +39 049 7923264; E-mail: massimo.zeviani@unipd.it

COXFA4; Zong *et al*, 2018). Yeast and mammalian COX species have been extensively studied during the last three decades and detailed structural data are now available. In contrast, COX composition and function in other eukaryotes has not been investigated in deep detail and the available information about the evolutionary conservation of the MRC complexes, and specifically of COX, is inferred by comparison of protein sequences. *Drosophila melanogaster* has been emerging as a suitable model organism for the study of mitochondrial biology and disease (Foriel *et al*, 2015, 2019; Brandt *et al*, 2017; Garcia *et al*, 2017; Thompson *et al*, 2018; Brischigliaro *et al*, 2019, 2021; Lieber *et al*, 2019; Murari *et al*, 2020; Scialò *et al*, 2020; Peruzzo *et al*, 2021). Therefore, it is important to define the detailed molecular composition and functional properties of the MRC complexes in this organism. For example, it is widely accepted that mammals and, more generally, the chordate *phylum* possess the largest version of COX, as specific subunits such as COX8A-C and COX7B are not found outside this *phylum*. Specifically, comparative analysis of COX protein sequences between *Homo sapiens* and *D. melanogaster* revealed the presence of 10 out of 11 homologous supernumerary COX subunits, with COX7B outstanding and therefore being considered the evolutionarily most recent subunit, as present only in vertebrates (Szuplewski & Terracol, 2001; Pierron *et al*, 2012; van Esveld & Huynen, 2018).

The “complexome profiling” method (Heide *et al*, 2012; Wittig & Malacarne, 2021; Cabrera-Orefice *et al*, 2022) consists of the separation of proteins in native polyacrylamide gels (Blue Native PAGE, BN-PAGE), coupled to mass spectrometry (MS) analyses of small consecutively cut gel slices. This technique has been exploited to determine the composition and distribution of the MRC complexes from different organisms (Heide *et al*, 2012; Kahlhöfer *et al*, 2017; Senkler *et al*, 2017; Evers *et al*, 2021; Pálenfková *et al*, 2021). We have applied complexome profiling to study the MRC of *D. melanogaster*. The profiles of COX subunit-derived peptide distribution allowed us to identify a novel protein physically associated with *D. melanogaster* COX, encoded by a gene of unknown function (CG7630). The CG7630 protein is indeed contained within the COX complexome-specific peak, together with all the canonical COX subunits, with the notable exception of the “missing” subunit, COX7B. CG7630 is unique to but invariantly present within protostome pluricellular organisms and we show here that its drastic knockdown *in vivo* leads to severe COX deficiency and ultimately developmental lethality. By combining structure prediction and homology modeling of the whole COX from *D. melanogaster* with complementation studies, we demonstrated that CG7630 is the invertebrate counterpart of COX7B.

In summary, we identified the allegedly missing COX subunit of pluricellular protostome invertebrates, that is, the functional ortholog of the vertebrate specific COX7B subunit, and showed that this subunit is essential for *D. melanogaster* COX activity. Our work demonstrates that, as in mammals, the protostome holoenzyme is in fact composed of 14 subunits and proves that complexome analysis and functional complementation, rather than just sequence similarity, are conclusive tools to establish the subunit composition of MRC complexes in different organisms.

Results

CG7630 encodes a putative novel COX subunit

To study the composition of *D. melanogaster* COX, we performed complexome profiling of digitonin-solubilized mitochondria from wild-type (w^{1118}) flies (Fig 1A). As shown in Fig 1B, the migration profiles and abundance, as displayed by heat maps, of all the known “canonical” COX subunits show co-migration in three main discrete peaks. The first, most abundant species, migrating at an apparent molecular mass of *ca.* 220 kDa, corresponds to the “monomeric” form of COX (IV₁). The second species (*ca.* 460 kDa) corresponds to the predicted molecular mass of the “dimeric” COX structure (IV₂). Finally, the third species, corresponding to a peak migrating at *ca.* 770 kDa, is the supercomplex IV+III₂ (Fig 1B). The core COX subunits annotated in FlyBase <https://flybase.org/reports/FBgg0000488.html>, that is, COX1, COX2, and COX3, as well as the supernumerary subunits COX4, COX5A, COX5B, levy/COX6A, COX6B, cype/COX6C, COX7A1, CG34172/COX7A2, and COX8, were all detected in our MS analysis. The only exception was COX7C, although the *D. melanogaster* proteome includes two polypeptides (COX7C and COX7CL) sharing high sequence identity with mammalian COX7C (35 and 46%, respectively). Notably, ND-MLRQ, the fly ortholog of mammalian NDUF4A, initially thought to belong to complex I (Carroll *et al*, 2006) but more recently demonstrated to be a COX subunit in mammals (Balsa *et al*, 2012; Pitceathly *et al*, 2013; Zong *et al*, 2018), co-migrates with the other COX subunits in our samples, confirming that the subunit is indeed a component of COX also in *D. melanogaster* (Garcia *et al*, 2017).

Hierarchical clustering of the complexome profiles, obtained from *D. melanogaster* mitochondria, revealed that two peptides that are part of a 90-amino acid protein product encoded by a gene with unknown function named CG7630 – FlyBase ID *FBgn0040793*, and located on chromosome 3, were consistently found in the same cluster containing the canonical COX subunits, (Fig 1B). The abundance profile of CG7630 showed a consistent co-migration pattern with all the identified COX subunits.

CG7630 is a *bona fide* COX subunit

Our results suggested that CG7630 is likely to be a previously uncharacterized COX supernumerary subunit. To further corroborate this hypothesis, we first tested whether CG7630 encodes a mitochondrially targeted protein. We expressed a C-terminal HA-tagged recombinant variant of CG7630 in *D. melanogaster* embryonic cells (S2R+), (Fig 2A), visualized its subcellular localization by immunofluorescence with anti-HA antibodies and compared its distribution with that of ATP5A (subunit alpha of ATP synthase, which is contained in mitochondrial cristae). As shown in Fig 2B, CG7630 unequivocally co-localized with the mitochondrial marker ATP5A, indicating that it is imported into the organelle. We then asked whether mitochondrial import of CG7630 depends on the presence of a mitochondrial targeting sequence (MTS). The analysis of CG7630 sequence with a mitochondrial prediction software, Mitofates (Fukasawa *et al*, 2015), identified a potential targeting sequence encompassing the first 23 N-terminal amino acids, with a putative cleavage site for the mitochondrial processing peptidase

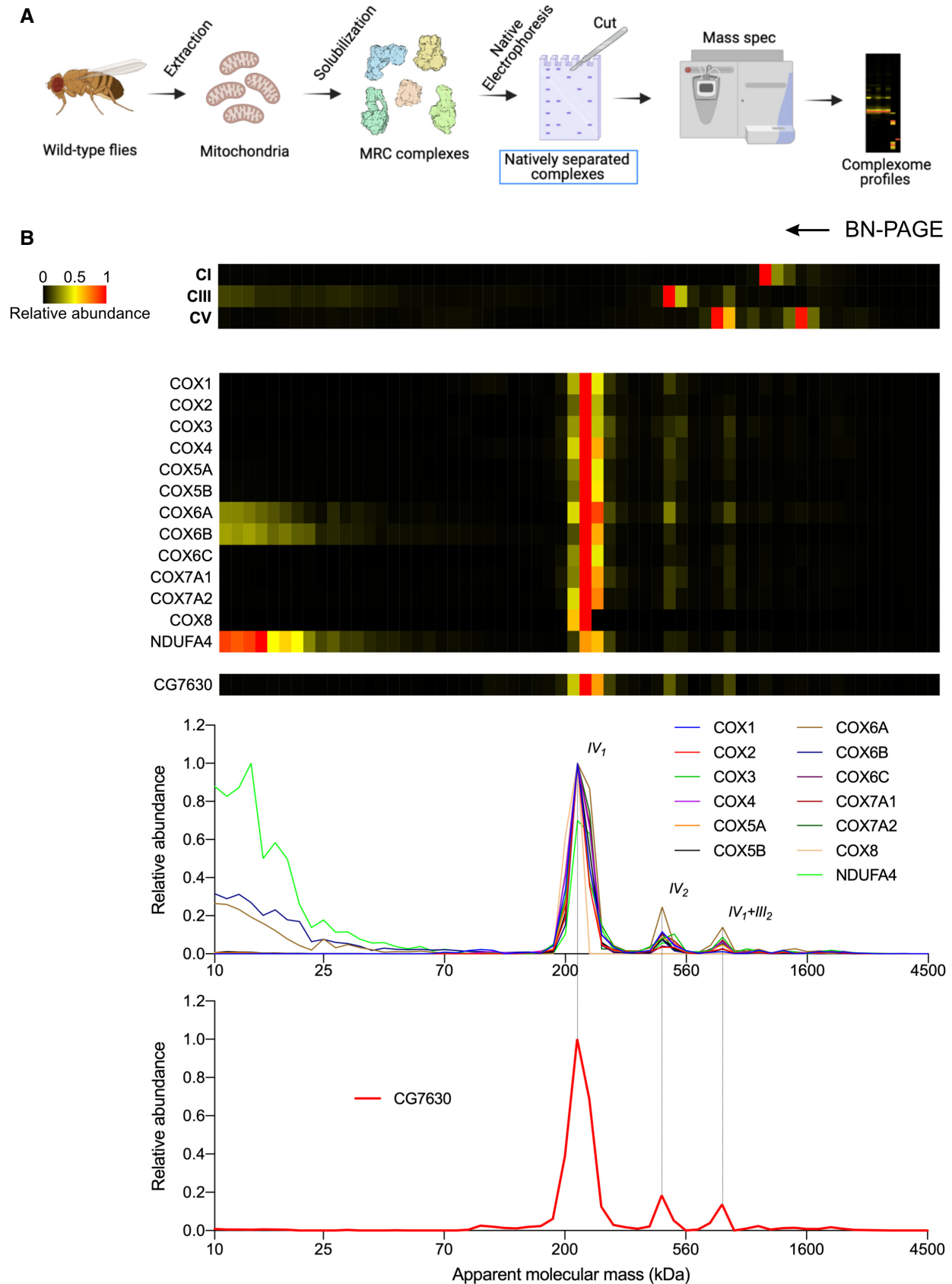


Figure 1.

Figure 1. Identification of CG7630 as a novel subunit of cytochrome c oxidase (COX).

- A Scheme of a complexome profiling experiment. Mitochondrial from adult *D. melanogaster* individuals were isolated and subjected to native electrophoresis after solubilization with a mild detergent (digitonin). Natively separated complexes were excised from the gel in 60 slices, each subjected to MS analysis. Peptide mass fingerprinting profile distribution throughout the gel lane was analyzed and shown as complexome profiles.
- B MS profiles depicted as heatmaps and relative abundance of MRC enzymes in natively separated complexes from wild-type fly mitochondria. Profiles of complexes I, III₂ and V (CI, CIII and CV) are reported as average migration profiles of their specific subunits identified by MS. Canonical COX subunits migrate as enzyme monomer (IV₁), dimer (IV₂) and together with dimeric complex III as supercomplex (IV₁ + III₂). A novel protein product of a gene with unknown function (CG7630) co-migrates with canonical COX subunits.

(MPP) at position 22. To understand whether CG7630 has a MTS, we generated synthetic protein constructs (Fig 2A). The deletion of amino acids 2–23 (CG7630^{Δ2–23}) abrogated the mitochondrial localization of CG7630-HA (Fig 2B). Moreover, fusion of the first 23 amino acids of CG7630 (CG7630^{1–23}) to a GFP reporter targeted the GFP to mitochondria (Fig 2B). These results confirmed that the N-terminus of CG7630 does contain a mitochondrial targeting sequence (MTS) consistent with results from MS analysis, which repeatedly detected two CG7630 tryptic peptides that correspond to the predicted mature part of the protein, encompassing amino acids 23–90.

To genetically test whether CG7630 encodes a subunit of COX, we knocked-down (KD) the expression of CG7630 *in vivo*, by expressing a 128-bp inverted repeat DNA sequence corresponding to a region of the CG7630 cDNA, through the GAL4/UAS system. We crossed the UAS responder fly line (CG7630^{RNAi}) with a strong ubiquitous driver line (*act5c-gal4*) to obtain RNAi progeny (*act5c-gal4*>CG7630^{RNAi}). Transgenic CG7630 KD individuals showed loss of *ca.* 80% of transcript expression measured by qPCR (Fig 3A). CG7630 KD progeny developed until the 3rd larval stage but eventually failed to reach pupation (Fig 3B and C). The developmental arrest correlated with severe reduction of COX activity in isolated mitochondria from CG7630 KD larvae, to approximately 55% of the controls (*act5c-gal4*>+, Fig 3D). CIII activity was slightly reduced as well (*ca.* 10%, Fig 3D) and CII activity was slightly increased (*ca.* 10%), possibly reflecting an induction of mitochondrial biogenesis, as frequently observed in human samples with COX deficiency (Brischiari & Zeviani, 2021). To investigate how the activity deficiency correlates with assembly defects of the enzyme, we solubilized mitochondria from CG7630 KD and control larvae with n-dodecyl-β-D-maltoside (DDM) and separated the MRC complexes by BN-PAGE. CI, CII, CIII, and CIV were specifically detected using either in-gel activity (IGA) assays or Western blot (WB) immune-visualization, using specific antibodies against one subunit for each complex. As shown in Fig 3E, IGA revealed strong reduction in the band corresponding to COX and a slight increase in succinate dehydrogenase (CII) activity, reflecting the spectrophotometric measurement of enzymatic activities. Additionally, WB immunodetection of COX from BN-PAGE using an antibody against the COX4 subunit showed that the decreased activity corresponded to severely reduced COX content in CG7630 KD mitochondria (Fig 3F). Conversely, no differences were observed for CI and CII, whereas CIII was marginally affected, in agreement with our kinetic measurements (Fig 3D). Notably, COX4 steady-state levels were also reduced by KD of CG7630 (Fig 3G), whereas other MRC complexes' subunits (SDHA, part of CII, and UQCR-C2, part of CIII) were unaffected.

To unequivocally demonstrate whether CG7630 is a *bona fide* COX subunit, we performed affinity purification of CG7630-HA

expressed in *D. melanogaster* S2R+ cells. As shown in Fig 3H, COX4 efficiently co-immunoprecipitated with affinity captured HA-tagged CG7630 under native conditions, whereas subunits of other MRC complexes, including NDUFS3 (CI), SDHA (CII), UQCR-C2 (CIII), and ATP5A (CV) failed to co-immunoprecipitate with CG7630-HA (Fig 3H).

Homology of CG7630 and COX7B

Using sequence-based methods, homologs of COX7B have been detected throughout the vertebrate lines, but not outside that *phylum* (van Esveld & Huynen, 2018). We used HHpred (Söding *et al.*, 2005; Hildebrand *et al.*, 2009), based on the prediction of functional-structural information according to comparisons based on hidden Markov modeling, to launch COX7B as a bait for screening the *D. melanogaster* proteome. Interestingly, we obtained CG7630 and gomdanji as the best hits ($E = 0.46$ and $E = 0.24$ respectively, Fig EV1). Furthermore, a reciprocal search with CG7630 against the human proteome detected COX7B as the best hit ($E = 3$). Notably, such E values are higher than the generally accepted cutoff scores for considering two proteins as homologous. However, as CG7630 and COX7B were clearly part of the same protein complex (COX), the E value could be lowered by a factor of ~1,000, making similarity highly significant. We failed to detect orthologs of gomdanji outside the *Drosophila* genus, and therefore, we did not analyze it further.

Phylogenetic distribution of CG7630/COX7B

Using Jackhmmer (Potter *et al.*, 2018), homologs of CG7630 can be detected in the major *taxa* of the protostome taxonomic branch for which genomes are available: *Arthropoda*, *Nematoda*, *Platyhelminthes*, *Mollusca*, *Tardigrada*, *Annelida*, *Bryozoa*, *Brachiopoda*, and *Rotifera*. CG7630 appears ubiquitous among the protostomes, as in more than 91% of the species that have a homolog of the well-conserved nuclear encoded subunit COX6A, we found a CG7630 homolog as well. Also, the CG7630 homologs were never lost in multiple species of a genus: that is, the absence of detectable homologs in a species appears to be due to incomplete genomes, gene prediction issues or undetectable homologs. We re-examined the phylogenetic distribution of COX7B, as homologs among the non-vertebrate *Deuterostomia* are undetected using Jackhmmer. We found a COX7B homolog in a nucleic acid sequence of the hemichordate *Saccoglossus kowaleski* (NCBI gene ID LOC100373479). Notably, although the two proteins are clearly distinct in *D. melanogaster*, we observed a number of instances in protostomes, where a homolog CG7630 is fused to the Apoptosis Inducing Factor (AIF) gene, for example, in Barnacles (A0A6A4VL42_AMPAM), Octopus (A0A7E6EJ31_OCTVU), and Daphnia (A0A0P5E3W8_9CRUS).

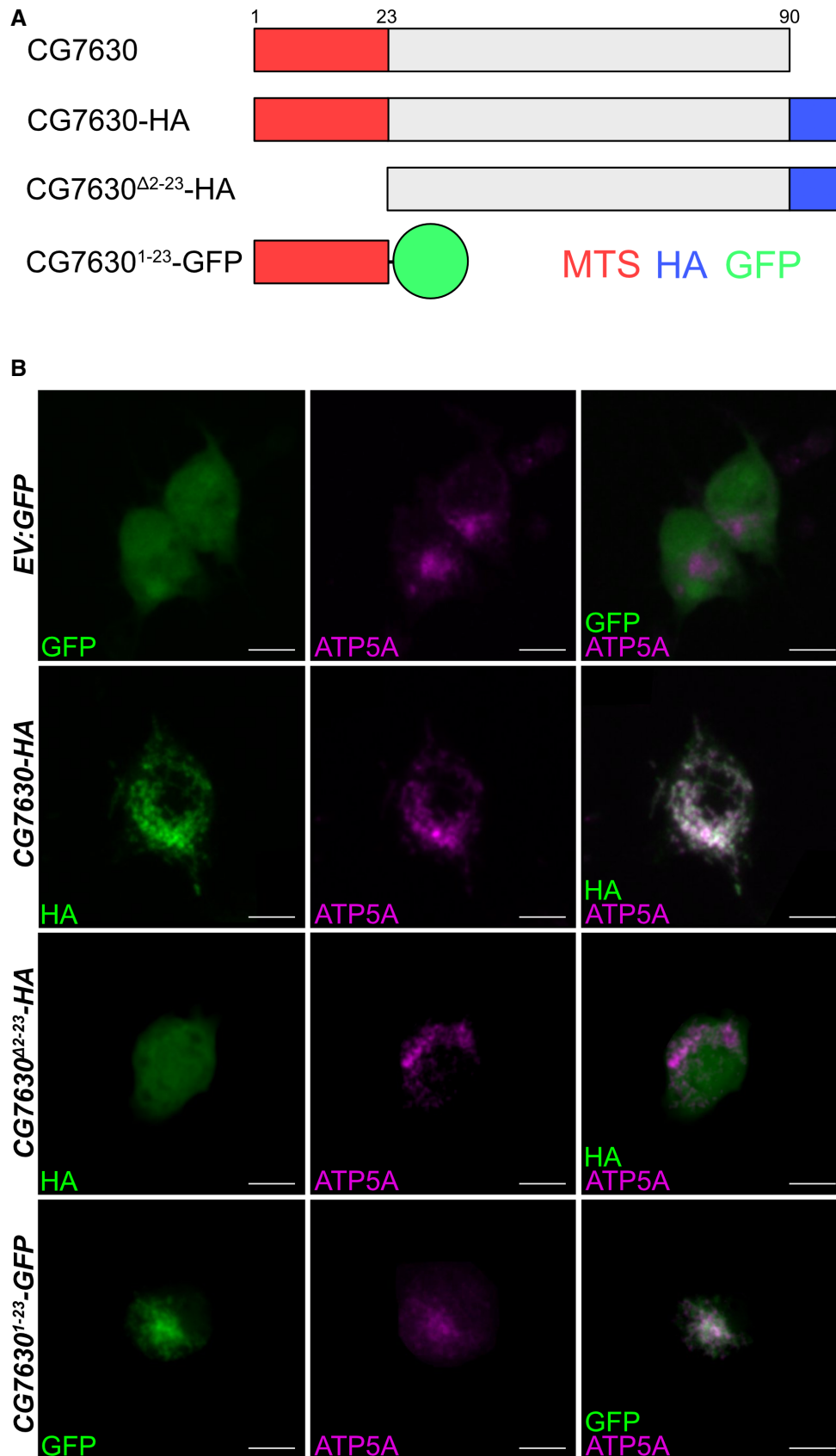


Figure 2.

Figure 2. CG7630 is a mitochondrial protein imported via an N-terminal MTS.

- A Scheme of synthetic constructs used to determine the subcellular localization of CG7630.
 B Confocal micrographs show the MTS-dependent mitochondrial localization of CG7630. Embryonic S2R+ cells were transfected with GFP-carrying the empty vector (EV:GFP), and vectors expressing HA-tagged CG7630 protein (CG7630-HA), a mutant CG7630-HA carrying a deletion in the putative MTS (CG7630^{Δ2-23}-HA) and a mutant consisting of CG7630 putative MTS fused with the GFP reporter (CG7630¹⁻²³-GFP). Scale bar: 5 μm.

Evolution of COX subunits

We established the presence of COX7B homologs in the two main branches of the *bilateria*: the *deuterostomia* (such as human and *S. kowaleski*) and the *protostomia* (such as *D. melanogaster*). This observation, combined with the absence of detectable homologs “pre-bilaterian” metazoan such as the *cnidaria* or the *porifera* argues for the origin of this subunit at the ancestral divergence point of *bilateria*. A number of other OXPHOS supernumerary proteins start appearing at the origin of *bilateria* (Fig 4A, Dataset EV1), including one other protein of the COX complex, COX8A (van Esveld & Huynen, 2018). Interestingly, COX8A and COX7B form two parallel TM helices close to each other at the same side of the COX complex (Zong *et al.* 2018), opposite the COX dimerization interface (Fig EV2). CG7630 contains, in contrast with COX7B, an insertion of ~20 amino acids at the N-terminus of the mature protein (Fig 4B) that would protrude into the matrix. This region is well conserved among its protostome homologs, including the gomdANJI protein and, together with the transmembrane (TM) helix, is annotated as the deltamethrin resistance domain. The name of that domain also found in gomdANJI protein is based on its presence in prag01, a protein associated with deltamethrin resistance in *Culex pipiens pallens* (Zhang *et al.* 2011). However, deltamethrin is not known to interact with COX.

Molecular modeling of *D. melanogaster* COX with CG7630

As no structural data for COX from any invertebrate animal are available, we used a hybrid strategy to generate a 3D model (Fig 5A–D) of the whole 14-subunit architecture of *D. melanogaster* COX including CG7630. Specifically, we combined structural homology data with high-resolution x-ray diffraction and cryo-EM reference structures of mammalian COX and artificial intelligence-based predictions from the AlphaFold database (Jumper *et al.* 2021; Varadi *et al.* 2022). As the remote homology detection based on HMMs profile comparison suggested the structure of bovine COX (PDB ID: 2Y69; Kaila *et al.* 2011) as the most suitable template for CG7630, we used this 13-subunit structure as the primary template. The cryo-EM structural information of human COX PDB ID 5Z62 (Zong *et al.* 2018) was used to recover NDUFA4/COXFA4 subunit (Pitceathly & Taanman, 2018). To obtain a model of the N-terminus of CG7630 (residues 23–51), that is missing in mammals, we included the coordinates obtained from AlphaFold predictions for this domain. The final model clearly retraces the typical COX topology and CG7630 obtained by the hybrid method nicely adapts to the holoenzyme (Fig 5A–D). The homologous region between COX7B and CG7630 covers the COX7B transmembrane helix and part of COX7B portion protruding into the intermembrane space (IMS). The TM segment of CG7630 is in close contact with COX4. The most conserved region is in the TM helix, mainly close to the matrix. Notably, in this segment of CG7630 a

pattern relevant for the interaction with COX4 can be identified, which is also present in COX7B (Fig 5E). Thus, the Asp56 in CG7630 can retain the H-bond interaction with the Lys75 of COX4, similar to the interaction of Asp39 and Lys101 in the human COX7B/COX4 bound structure. In *D. melanogaster*, this interaction could be even more strongly stabilized by the presence of a second Asn in position 52, the sidechain of which is still orientated toward Lys75 (Fig 5E). Likewise, the hydrophobic residue Leu59, also facing COX4, is preserved (corresponding to Leu42 in COX7B, Fig 5E). The closest point between the TM domains of CG7630 and COX4 occurs at position Gly62 of CG7630 (corresponding to Gly45 in COX7B) is necessary to maintain the appropriate distance as the absence of the sidechain is likely to favor the helix contacts (Fig 5E).

Human COX7B can rescue COX deficiency in *D. melanogaster* cells

To determine whether CG7630 and human COX7B (hCOX7B) are in fact orthologs, we performed functional complementation assays. We generated stable S2R+ *D. melanogaster* cell lines carrying the pAc5-STABLE2-neo vector in which we cloned C-terminally HA-tagged forms of either CG7630 or hCOX7B. Then, we performed targeted RNAi via soaking cultured cells with synthetic dsRNAs (Clemens *et al.* 2000) targeting CG7630, which induced > 95% reduction of the CG7630 transcript in wild-type S2R+ cells (Fig 6A). Then, we checked the expression of rescue constructs in CG7630 KD cells. hCOX7B-HA and CG7630-HA transcripts were expressed (Fig 6B) and translated into proteins (Fig 6C). The expression of CG7630 transcript in cells carrying the CG7630-HA construct was 5-fold higher than that of cells carrying the empty vector (EV), and therefore expressing only endogenous CG7630. In CG7630-HA expressing cells, exposure to dsRNA against CG7630 reduced transcript levels of CG7630 (Fig 6B), which, however, remained still 2.6-fold higher than those found in the EV control cells treated with mock dsRNA. Accordingly, CG7630-HA levels were decreased in KD cells vs. non-KD CG7630-HA expressing cells (Fig 6C). When we measured COX activity in the EV control S2R+ cells exposed to dsRNA, we found that the KD of CG7630 suppressed COX activity by ~60% (Fig 6D). Expression of CG7630-HA in these very cells determined a recovery of COX activity to values virtually identical to those of the EV, mock-treated control cells (Fig 6D). Notably, when hCOX7B-HA was expressed in fly cells in which the expression of CG7630 was knocked-down, COX activity was significantly increased, reaching levels of ~70% of the mock-treated control (EV) cells (Fig 6D). In addition, we tested the steady-state levels of CI, CII, CIV, and CV subunits from whole-cell lysates, separated by SDS-PAGE, and immunovisualized by WB with specific antibodies. As shown in Fig 6E, ATP5A (CV subunit) and SDHA (CII subunit) levels were affected neither by CG7630 KD nor by CG7630 or COX7B expression. Conversely, the COX4 immunoreactive band was severely reduced by CG7630 KD in EV cells.

Again, the expression of hCOX7B partially rescued the levels of COX4 in *CG7630* KD cells (Fig 6E), whereas full rescue, comparable to the levels found in mock-treated control EV cells, was obtained in *CG7630-HA* expressing cells. Taken together, these results demonstrated that the *CG7630* protein is a necessary component for COX assembly and function in *D. melanogaster*, where it clearly plays the same role established in mammalian COX by COX7B.

Discussion

The MRC of eukaryotes derives from evolutionary remodeling of minimal enzymatic units found in prokaryotes (Pereira *et al*, 2001; Esposti, 2020). Thus, it is currently well accepted that MRC complexes acquired more and more subunits and increased their complexity throughout evolution, with vertebrates and, more specifically, mammals having the largest and most multiheteromeric

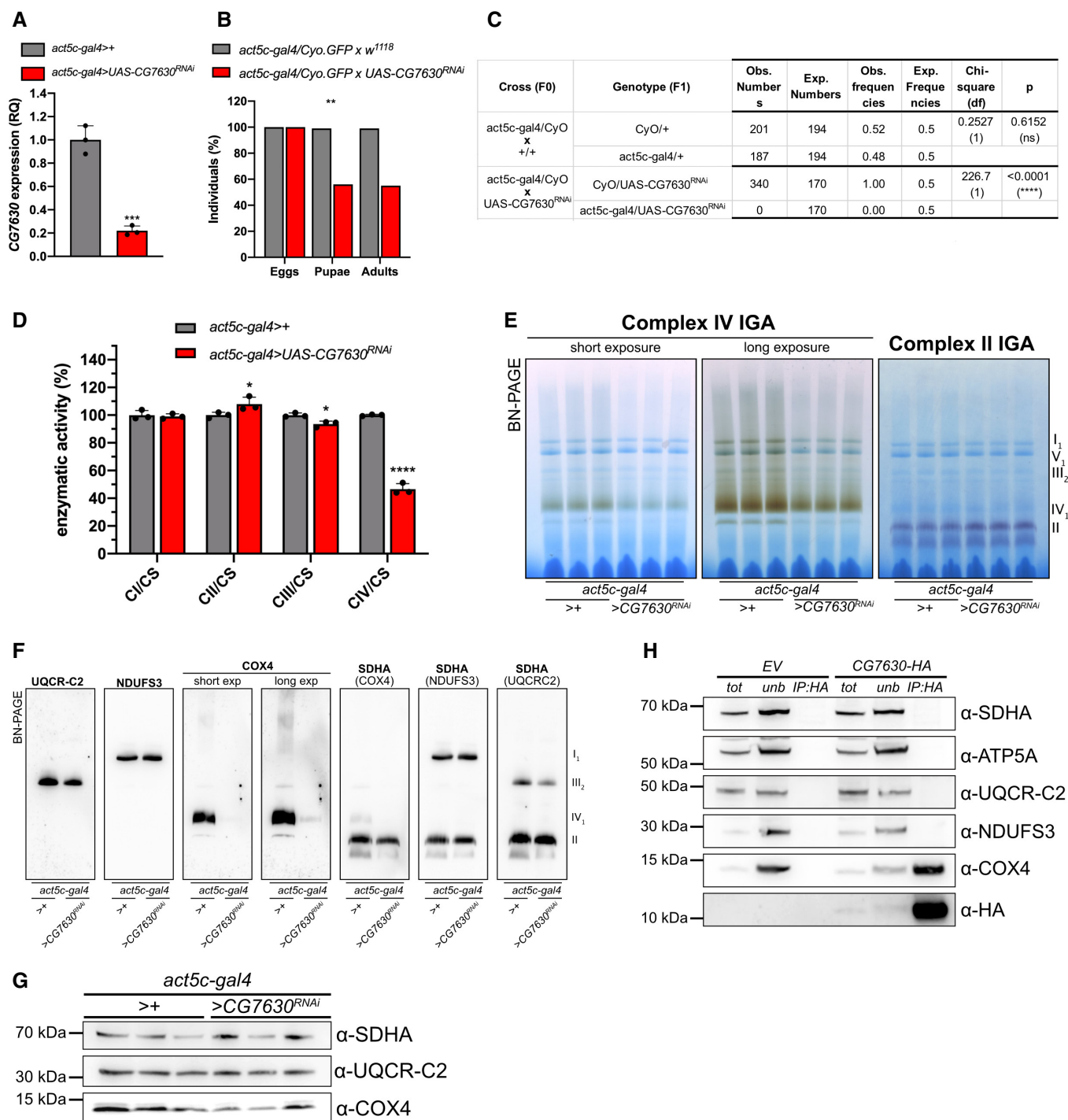


Figure 3.

Figure 3. CG7630 is a bona fide COX subunit.

- A Relative quantification (RQ) of *CG7630* transcript after RNAi with a 120-bp inverted-repeat sequence (*act5c-gal4>UAS-CG7630^{RNAi}*) compared to control (*act5c-gal4>+*). Data are plotted as mean \pm SD ($n = 3$ biological replicates, Student's *t* test $***P = 0.0005$).
- B Relative percentage of egg to adult viability of *CG7630* RNAi cross (*act5c-gal4/CyO.GFP x UAS-CG7630^{RNAi}*) and control cross (*act5c-gal4/CyO.GFP x w¹¹¹⁸*), calculated at three developmental stages (eggs, pupae, and adults), ($n > 250$, Chi-square test 9.920 df(2), $**P = 0.007$).
- C Mendelian frequencies of adults obtained by crossing heterozygous *act5c-gal4>CyO.GFP* flies with *w¹¹¹⁸* genetic background flies (+/+) ($n = 388$ individuals, Chi-square test 0.2527, df(1), $P = 0.6152$), and by crossing heterozygous *act5c-gal4>CyO.GFP* flies with homozygous *UAS-CG7630^{RNAi}* flies ($n = 340$ individuals, Chi-square test 226.7, df(1), $****P < 0.0001$).
- D Kinetic enzyme activity of individual MRC complexes in *CG7630* RNAi and control individuals normalized by citrate synthase (CS) activity. Data are plotted as mean \pm SD ($n = 3$ biological replicates, two-way ANOVA with Sidak's multiple comparisons, $*P \leq 0.05$, $****P \leq 0.0001$).
- E In gel-activity assays for MRC complexes II and IV in DDM-solubilized mitochondria from RNAi (*act5c-gal4>UAS-CG7630^{RNAi}*) and control larvae (*act5c-gal4>+*).
- F BN-PAGE, Western blot immunodetection of MRC complexes from *CG7630* RNAi (*act5c-gal4>UAS-CG7630^{RNAi}*) and control (*act5c-gal4>+*) larvae using antibodies against specific subunits: anti-UQCRC2 (complex III), anti-NDUF53 (complex I), anti-COX4 (complex IV) and anti-SDHA (complex II).
- G Western blot analysis of steady-state levels (SDS-PAGE) of MRC subunits COX4 (complex IV), SDHA (complex II) and UQCR-C2 (complex III) in whole lysates from *CG7630* RNAi (*act5c-gal4>UAS-CG7630^{RNAi}*) and control (*act5c-gal4>+*) larvae.
- H Western blot analysis of anti-HA affinity purified samples from S2R+ *D. melanogaster* cells. EV = samples from cells carrying the empty expression vector. *CG7630-HA* = samples from cells expressing HA-tagged *CG7630*. Tot = total mitochondrial-enriched fractions; *unb* = unbound material; *IP:HA* = immunoprecipitated material. Samples were probed with antibodies against MRC subunits of complexes I (NDUF53), II (SDHA), III (UQCR-C2), IV (COX4), and V (ATP5A).

Source data are available online for this figure.

enzymes (Szuplewski & Terracol, 2001; Pierron *et al*, 2012; van Esveld & Huynen, 2018), although also the apicomplexa *Plasmodium falciparum* and *Toxoplasma gondii* have acquired a large set of new accessory subunits (Evers *et al*, 2021; Maclean *et al*, 2021). Detailed information about the functional or structural role of each of the COX supernumerary subunits is still lacking (Čunátová *et al*, 2020). The most studied subunit is COX4, for which it has been proposed a modulatory role in oxygen affinity in different tissues or under different energetic demands and oxygen availability (Fukuda *et al*, 2007; Hüttemann *et al*, 2007; Acin-Perez *et al*, 2011; Pajuelo Reguera *et al*, 2020). Mammalian COX is considered the largest CIV species in metazoans, having one specific subunit—COX7B—that was never identified outside vertebrates due to lack of sequence homology.

Here, we prove that this widely accepted concept is incorrect. We provide compelling evidence that invertebrate COX is composed of 14 subunits, as the mammalian enzyme, and that an evolutionary divergent protein with a non-conserved amino acid sequence plays the same structural and functional role of mammalian COX7B. Specifically, by applying complexome profiling to *D. melanogaster* mitochondria, we identified a protein of previously unknown function, showing an identical migration profile to canonical COX subunits. This protein is encoded by an uncharacterized gene—*CG7630*—and is targeted to mitochondria through a canonical N-terminal mitochondrial targeting sequence (MTS) which appears to be cleaved off the mature protein, according to our proteomic data. This suggests that the protein is processed by the mitochondrial matrix protein, as a canonical structure eventually targeted to the inner mitochondrial membrane.

We showed that the knockdown of *CG7630* *in vivo* leads to developmental arrest at the larval stage in *D. melanogaster* linked with severe reduction in COX enzyme activity, demonstrating that *CG7630* encodes a bona fide COX subunit.

The only COX subunit missing in the *D. melanogaster* proteome was COX7B. Although *CG7630* and human COX7B have low sequence similarity, we demonstrate that, by biocomputational reconstruction, they share homology in secondary and tertiary structures (e.g., the hydrophobic TM-helix) and possess conserved residues needed for docking its unique interactor, subunit COX4, in a

manner similar to COX7B. Moreover, the fact that human COX7B is able to rescue defects in *CG7630* KD cells conclusively proves that *CG7630* and COX7B are functional orthologs.

This work demonstrates that vertebrate and protostome COX complexes are structurally identical and that COX7B should not be considered as a functionally and structurally unique acquisition of the most recent animal phylum, vertebrates, but a homolog in deuterostomes of a subunit which is also present in protostomes. Whether COX7B confers additional, or specific, regulatory functions to the enzyme in vertebrates, including mammals, is still unknown. Likewise, the evolutionary mechanisms and possible functional implications of the divergence between the two “COX7B orthologs” in the two divisions of *bilateria* are unresolved issues. Unquestionably, this subunit has a relevant physiological and pathological role, since mutations in *COX7B* have been found in patients who suffer from mitochondrial disease with COX deficiency (Indrieri *et al*, 2012) and the knockdown of *CG7630* is clearly deleterious for the COX activity in, and the development of, *D. melanogaster*. Indeed, *CG7630* species appear to play the same role in pluricellular invertebrate animals as COX7B in chordates, the two superphyla of *bilateria*. For this reason, we propose to rename *D. melanogaster* *CG7630* as COX7B-like protein (COX7BL).

Intriguingly, among the homologs of *CG7630* in other protostomes, we observed proteins fused to an Apoptosis Inducing Factor (AIF). Consistent with the intermembrane space location of the AIF protein (Otera *et al*, 2005), the gene is fused with the C-terminus of the *CG7630* homolog, which is predicted to be in the intermembrane space. Remarkably, a very recent work showed that around 10% of mammalian COX interacts with AIF (Hevler *et al*, 2021). Our findings support the hypothesis that the fusion protein formed by the ortholog of *CG7630*+AIF, detected in some protostomes, has a functional role, which is carried out in deuterostomes by COX7B interacting with, but physically separated from AIF. It is likely, but still unproven, that the same interaction may occur between *CG7630* and AIF, also in those protostome organisms, such as *D. melanogaster*, in which the two proteins are clearly distinct. Our work provides additional support to a newly identified and still unsolved functional partnership between COX and AIFM1-encoded proteins whose physiological and pathological relevance will be investigated in the future.

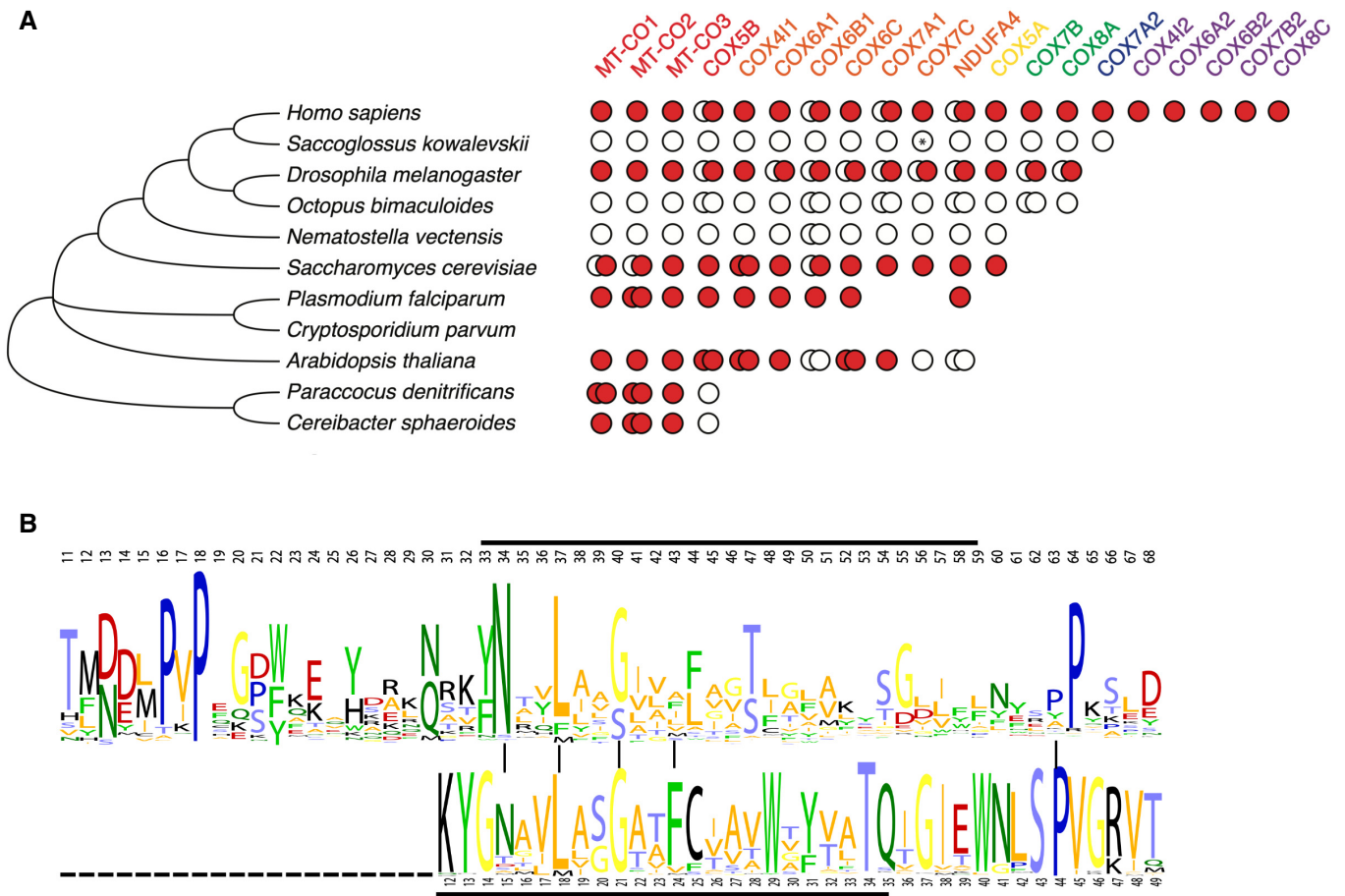


Figure 4. Phylogenetic distribution of CG7630/COX7B suggests it emerged at the root of bilateria.

- A** Scheme of the evolution of subunits part of human cytochrome c oxidase, sorted by their evolutionary origin, with the oldest subunits on the left. Subunits colored in red date back to bacteria. Orange indicates subunits with a common ancestor at the root of eukaryotes. Subunits shared between animals and fungi (opisthokonts) are in yellow while subunits dating at the origin of bilateria are in green. Blue is for the subunit that can be traced back to the deuterostomia and purple is for the subunits originated after the origin of deuterostomia. Note that the most recent subunits originate from gene duplications.
- B** Alignment of the sequence logos of COX7B and CG7630. The sequence logos were created with weblogo (<https://weblogo.berkeley.edu/>) using alignments obtained from JackHMMER. The positions that are conserved between the profiles (Fig EV1) are indicated with vertical lines, and the (predicted) TM helix is indicated with a horizontal line. The amino acid positions are based on the mature protein. Relative to COX7B, CG7630 has a 20 amino acid insertion close to the N terminus of the mature protein.

Our work provides a clear example of the power of proteomic approaches, such as complexome profiling, to overcome limitations given by evolutionary protein sequence divergence that add to the complexity of the MRC. Further work is warranted to deeply investigate and characterize the composition of all the respiratory complexes in standard invertebrate model—*D. melanogaster*—to help clarify MRC subunit composition and distribution throughout evolution.

Materials and Methods

Fly stocks and maintenance

Flies were raised on standard cornmeal medium and kept at 23°C, 70% humidity on a 12:12 h light/dark cycle. Fly strains used in this study were obtained from Bloomington Drosophila Stock Center (BDSC) and Vienna Drosophila Resource Center (VDRC). Genotypes

used in this study were: *w¹¹¹⁸* (BDSC), *act5c-gal4>CyO.GFP* (BDSC 4414) and *UAS-CG7630-IR* (VDRC 107667). Control individuals were obtained by crossing the *gal4* driver line with the genetic background flies *w¹¹¹⁸*.

Isolation of mitochondria

Mitochondria from *D. melanogaster* larvae were prepared by differential centrifugation as described previously (Brischigliaro et al, 2022). Protein concentration of mitochondrial extracts was measured with the Bradford method (Bio-Rad protein assay).

Complexome profiling

Isolated mitochondria were pelleted by centrifugation and the supernatant was discarded. Mitochondrial proteins (0.2 mg) were solubilized with 6 g digitonin/g protein in 50 mM NaCl, 5 mM

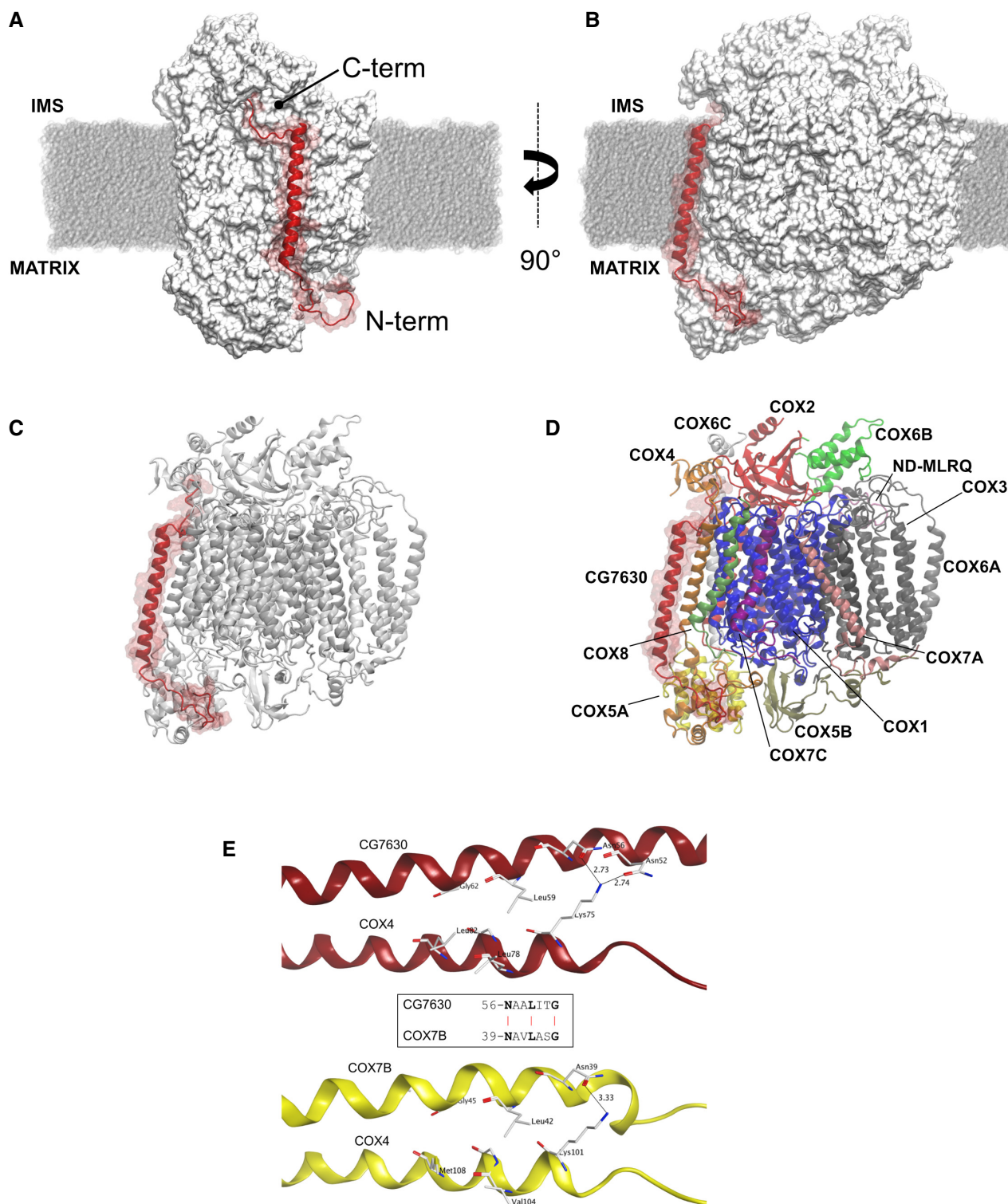


Figure 5. The 14-subunit model of *Drosophila melanogaster* COX enzyme.

- A, B The front and side view of CG7630, panel (A and B), respectively, is reported using the red ribbon and its molecular surface is in transparent red against the other COX subunits in gray-white. The inner mitochondrial membrane is reported in dark gray.
- C In panel C, the ribbon representation is extended to the whole enzyme.
- D In panel D, each subunit is shown as a ribbon in different colors.
- E Panel E shows *Drosophila melanogaster* atomic model of CG7630 and COX4 helices (red) interactions compared to the human COX7B-COX4 interactions (yellow). The conserved residues, located in the proximity of the intermembrane space and involved the helix-helix interactions, are highlighted using stick representation and the distance of the observed H-bonds are displayed.

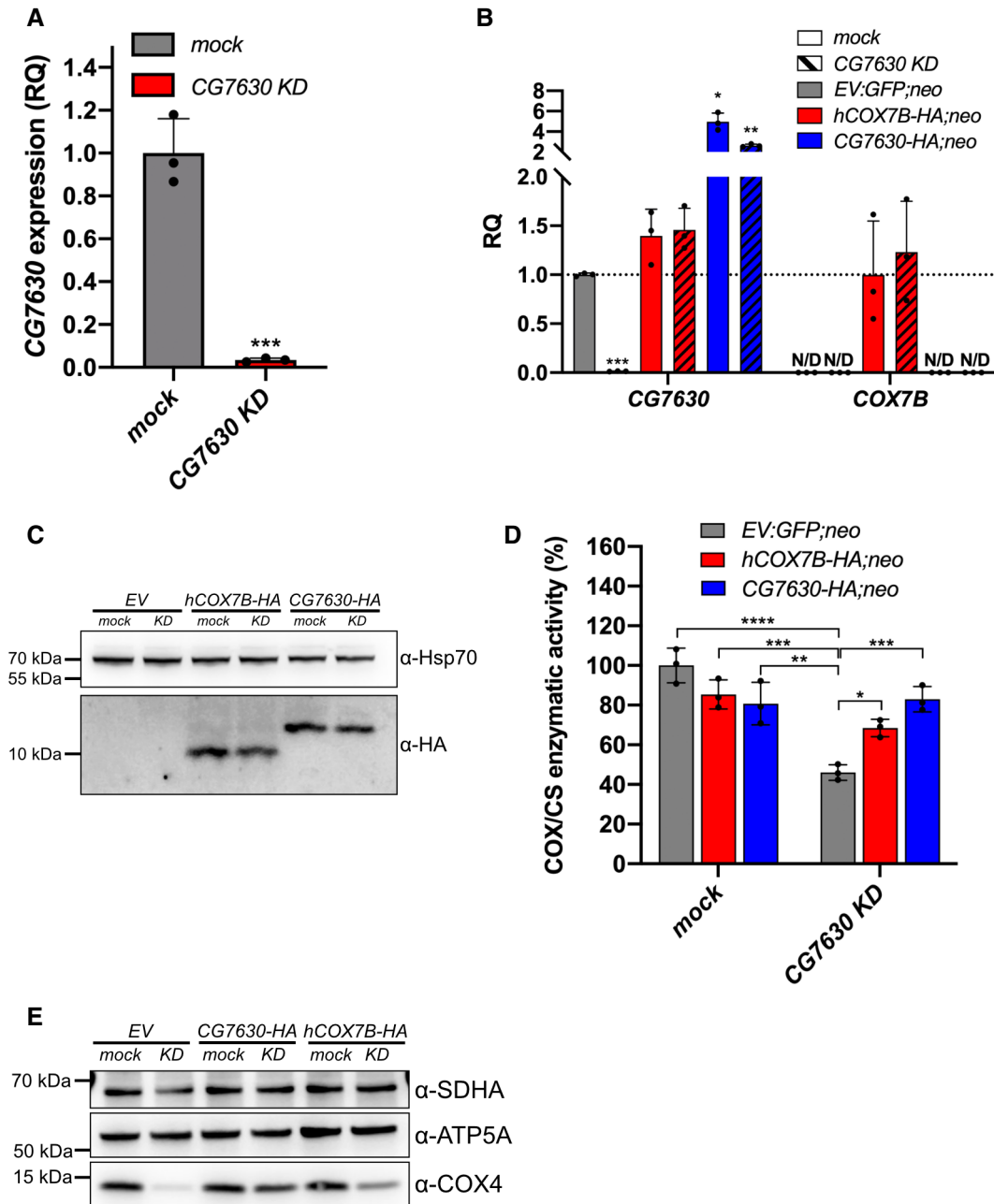


Figure 6. Human COX7B can rescue COX deficiency caused by loss of CG7630.

- A** Relative quantification (RQ) of *CG7630* transcript in wild-type *D. melanogaster* S2R+ cells treated with a dsRNA targeting *CG7630* (*CG7630 KD*) and a mock control dsRNA (*mock*). Data are plotted as mean \pm SD ($n = 3$ biological replicates, Student's *t* test **** $P = 0.0005$).
- B** Relative quantification (RQ) of *CG7630* and *COX7B* transcripts in stable S2R+ cell lines carrying the empty expression vector (*EV:GFP;neo*), and expression vectors carrying HA-tagged forms of human COX7B (*hCOX7B-HA;neo*) and CG7630 (*CG7630-HA;neo*). Cells were treated with a dsRNA targeting *CG7630* (striped bars, *CG7630 KD*) and a mock control dsRNA (solid bars, *mock*). N/D = not detected. Data are plotted as mean \pm SD ($n = 3$ biological replicates, one-way ANOVA with Dunnett's multiple comparisons, * $P = 0.0370$, ** $P = 0.0074$, *** $P = 0.0003$).
- C** Immunoblot analysis of stable S2R+ cell lines carrying the empty expression vector (*EV:GFP;neo*), and expression vectors carrying HA-tagged forms of human COX7B (*hCOX7B-HA;neo*) and CG7630 (*CG7630-HA;neo*). The *CG7630* transcript was knocked-down (*KD*) in cells by a dsRNA targeting *CG7630* and compared with cells treated with a mock control dsRNA (*mock*). Samples were probed with an antibody anti-HA tag and with an antibody against Hsp70 as an endogenous control.
- D** Kinetic enzyme activity of COX normalized by citrate synthase activity (CS) in stable S2R+ cell lines carrying the empty expression vector (*EV:GFP;neo*), and expression vectors carrying HA-tagged forms of human COX7B (*hCOX7B-HA;neo*) and CG7630 (*CG7630-HA;neo*). Cells were treated with a dsRNA targeting *CG7630* (striped bars, *CG7630 KD*) and a mock control dsRNA (solid bars, *mock*). Data are plotted as mean \pm SD ($n = 3$ biological replicates, two-way ANOVA with Sidak's multiple comparisons, * $P \leq 0.05$, ** $P \leq 0.01$, *** $P \leq 0.001$, **** $P \leq 0.0001$).
- E** Steady-state levels of MRC subunits in samples from rescue experiment performed as in (D).

Source data are available online for this figure.

6-aminohexanoic acid, 1 mM EDTA, 50 mM imidazole/HCl, pH 7.0. After centrifugation at $22,000 \times g$ for 20 min at 4°C , the supernatant was supplemented with Coomassie brilliant blue G250 and proteins were separated by 4–16% gradient BN-PAGE. Digitonin-solubilized mitochondrial proteins from bovine heart were loaded as molecular mass standards. After electrophoresis, the gel was fixed and stained with Coomassie blue. Gel lanes were cut into 60 even pieces, each of which was cut into smaller pieces, transferred to a 96-well filter microtiter plate (Millipore), and destained in 50% (v/v) methanol, 50 mM ammonium bicarbonate. After complete destaining, in-gel digestion with trypsin was performed. Tryptic peptides were separated by liquid chromatography and analyzed by tandem mass spectrometry (LC-MS/MS) in a Q-Exactive 2.0 Orbitrap Mass Spectrometer (2.8 SP1) equipped with an Easy nLC1000 nano-flow ultra-high-pressure liquid chromatography system (Thermo Fisher Scientific) at the front end. Thermo Scientific Xcalibur 3.1 Software Package was used for data recording. Mass spectrometry RAW data files were analyzed using MaxQuant (version 1.5.0.25). The extracted spectra were matched against the *D. melanogaster* Uniprot Reference Sequence database (release 2020_04). Database searches were done with 20 ppm match tolerances. Trypsin was selected as the protease with two missed cleavages allowed. Dynamic modifications included N-terminal acetylation and oxidation of methionine. Cysteine carbamidomethylation was set as a fixed modification. Keratins, known contaminants, and trypsin were removed from the list. The abundance of each protein was determined by label-free quantification using the composite intensity based absolute quantification (iBAQ) values determined by MaxQuant analysis and was corrected for loading and MS sensitivity variations between samples based on the total iBAQ value for all detected complex V

subunits. Gel migration profiles were created for each protein and normalized to the maximum abundance. The profiles of the identified mitochondrial proteins were hierarchically clustered by distance measures based on Pearson correlation coefficient (uncentered) and the average linkage method using the NOVA software package v0.5 (Giese *et al*, 2015). The visualization and analysis of the heatmaps representing the normalized abundance in each gel slice by a three-color code gradient (black/yellow/red) were made using Microsoft Excel 2019 and Graph Pad Prism 8.4.3. The mass calibration for the BN-PAGE gels was performed as previously described (Guerrero-Castillo *et al*, 2017). Membrane proteins were calibrated using the well-known molecular masses of respiratory chain complexes and supercomplexes from bovine heart mitochondria. The soluble proteins were, however, calibrated using the following set of *Drosophila* proteins: ATPB (51 kDa), malate dehydrogenase (72 kDa, dimer), citrate synthase (100 kDa, dimer), ETFA/B (122, heterodimer), heat shock protein 60 (410 kDa, heptamer), ALDH7A1 (675 kDa, dodecamer).

RNA isolation, reverse transcription, and qRT-PCR

Total RNA was extracted from 10 larvae for each genotype using TRIzol method (Thermo Fisher Scientific) according to the manufacturer's instructions. Reverse transcription was performed with the GoScript Reverse Transcriptase kit (Promega). qRT-PCRs were performed using GoTaq qPCR SYBR Green chemistry (Promega) and a Bio-Rad CFX 96 Touch System (Bio-Rad). The $2^{-\Delta\Delta C_t}$ method (relative quantification) was used to calculate the expression levels of the targets using *Rp49* as endogenous control. The oligonucleotides used in this study are listed in the table of primers (Table 1).

Table 1. List of oligonucleotides used in this study.

Name	Sequence (5'–3')
CG7630_qPCR_F	CGCTCACTACTGGCATTCT
CG7630_qPCR_R	GGATGATACCAGAAGATTTCCAG
Rp49_qPCR_F	ATCGGTTACGGATCGAACA
Rp49_qPCR_R	GACAATCTCCTTGCCTTCT
COX7B_qPCR_F	TTCCCTTGGTCAAAGCGCA
COX7B_qPCR_R	GGTGTACGTTTCTGGTGGCT
dsRNA_CG7630_F	TTAATACGACTCACTATAGGGAGATGACTTACCACGGTGGACATGG
dsRNA_CG7630_R	TTAATACGACTCACTATAGGGAGAATGGGACGAGAATGCCAGTATGATG
dsRNA_mock_F	TTAATACGACTCACTATAGGGAGATGTAGACAATGGCGATGACCACTC
dsRNA_mock_R	TTAATACGACTCACTATAGGGAGAATGGTTTCTGCGGTGTTGGAG
CG7630_pAc5_EcoRI_F	CAGTGTGGTGAATTCCAAAATGTTGGTTAAGCACATTGTC
CG7630-HA_pAc5_HindIII_R	CTCTGCCCTCAAGCTTTTAAGCGTAATCTGGAACATCGTATGGGTAGTCCAGGCTCTTGGGCGC
CG7630- Δ MTS_pAc5_EcoRI_F	CAGTGTGGTGAATTCCAAAATGTACCACGGTGGACATGGTCC
CG7630MTS-GFP_pAc5_XbaI_R	CCATGGTGGCTCTAGAAGCGGCACCGCACAAAGC
COX7B_pAc5_EcoRI_F	CAGTGTGGTGAATTCCAAAATGTTCCCTTGGTCAAAGCGC
COX7B-HA_pAc5_HindIII_R	CTCTGCCCTCAAGCTTTTAAGCGTAATCTGGAACATCGTATGGGTACTGATTCTCCATTCTTTGGG
CG7630-HA_pAc5_HindIII_R_neo	CTCTGCCCTCAAGCTTAGCGTAATCTGGAACATCGTATGGGTAGTCCAGGCTCTTGGGCGC
COX7B-HA_pAc5_HindIII_R_neo	CTCTGCCCTCAAGCTTAGCGTAATCTGGAACATCGTATGGGTACTGATTCTCCATTCTTTGGG

Table 2. List of antibodies used in this study.

Antibody	Source	Cat. No./Ref	Application	Concentration
Mouse monoclonal anti-NDUFS3	Abcam	ab14711	WB	1:1,000
Rabbit polyclonal anti-COXIV	Cell Signaling Technology	4844	WB	1:1,000
Mouse monoclonal anti-ATP5A	Abcam	ab14748	IF	1:200
Mouse monoclonal anti-Hsp70	Sigma-Aldrich	H5147	WB	1:1,000
Rabbit monoclonal anti-HA	Cell Signaling Technology	3724	WB, IF	1:1,000, 1:300
Rabbit polyclonal anti-UQCR-C2	Dr. Edward Owusu-Ansah	Murari et al (2020)	WB	1:2,000
Rabbit polyclonal anti-Sdha	Dr. Edward Owusu-Ansah	Murari et al (2020)	WB	1:2,000
Goat anti-Mouse IgG	Promega	W402B	WB	1:5,000
Goat anti-Rabbit IgG	Promega	W401B	WB	1:3,000
Goat anti-rabbit Alexa Fluor 488	Thermo Fisher Scientific	A11008	IF	1:100
Goat anti-mouse Alexa Fluor 647	Thermo Fisher Scientific	A32728	IF	1:200

Blue-native polyacrylamide gel electrophoresis (BN-PAGE) and in-gel activity (IGA) assays

Isolated mitochondria were resuspended in 1.5 M aminocaproic acid, 50 mM Bis-Tris/HCl pH 7.0. The samples were solubilized with 4 mg of n-dodecyl- β -D-maltoside (Sigma) per mg of protein. After 5 min of incubation on ice, samples were centrifuged at $18,000 \times g$ at 4°C for 30 min. The supernatant was collected and resuspended with Sample Buffer (750 mM aminocaproic acid, 50 mM Bis-Tris/HCl pH 7.0, 0.5 mM EDTA and 5% Serva Blue G). Native samples were separated using NativePAGE 3–12% Bis-Tris gels (Thermo Fisher Scientific) according to the manufacturer's protocol.

For the detection of the activity of mitochondrial respiratory chain complexes, gels were stained with the following solutions. Complex II (succinate dehydrogenase): 5 mM Tris-HCl pH 7.4, 0.2 mM phenazine methosulfate (Sigma), 20 mM succinate, and 1 mg/ml nitrotetrazolium blue chloride; Complex IV (cytochrome c oxidase): 50 mM potassium phosphate pH 7.4, 1 mg/ml 3',3'-diaminobenzidine tetrahydrochloride hydrate (Sigma), 24 units/ml catalase from bovine liver (Sigma), 1 mg/ml cytochrome c from equine heart (Sigma), and 75 mg/ml sucrose.

Analysis of MRC activity

The activities of mitochondrial respiratory chain complexes and citrate synthase (CS) were measured by spectrophotometry, as described previously (Brischiaglio et al, 2022).

Western blot and immunodetection

BN-PAGE gels were transferred to PVDF membranes in Dunn carbonate buffer (10 mM NaHCO₃, 3 mM Na₂CO₃) applying a constant voltage of 25 V at 4°C for 1 h using a XCell II™ Blot Module (Thermo Fisher Scientific). SDS-PAGE gels were transferred to PVDF membranes in Tris-Glycine transfer buffer (25 mM Tris-HCl, 192 mM Glycine, 20% methanol, 0.025% SDS) applying a constant voltage of 100 V at 4°C for 1 h using a Mini Trans-Blot® Cell (Bio-Rad). For the immunodetection of specific protein targets, blotted PVDF membranes were blocked in 5% skimmed milk in PBS-T (0.1% Tween-20) at room temperature for 1 h and then incubated overnight with

primary antibodies diluted in 3% BSA in PBS-T overnight at 4°C. After incubating the primary antibody, the PVDF membranes were washed three times with PBS-T for 10 min, incubated with the secondary HRP-conjugated antibody for 1 h at room temperature and washed three times with PBS-T for 10 min. Chemiluminescent signals were recorded using an Alliance Mini HD9 (UVITEC). Antibodies used are listed in the table of antibodies (Table 2).

Cell cultures and molecular cloning

The *Drosophila* S2R+ cell line is derived from a primary culture of late stage (20–24 h old) *D. melanogaster* embryos and was obtained from the *Drosophila* Genomics Resource Center (DGRC ID 150). S2R+ cells grow at 25°C without CO₂ in Schneider's medium (Biowest) with 10% heat-inactivated fetal bovine serum (FBS; Euroclone). *CG7630* and *COX7B* cDNAs were cloned in pAc5-STABLE2-neo vector (González et al, 2011) using In-Fusion HD cloning kit (Takara Bio) according to the manufacturer's instructions. Primers used for molecular cloning are listed in the table of primers (Table 1).

Co-immunoprecipitation

Mitochondrial-enriched fractions from S2R+ cells were solubilized under native conditions on ice for 10 min using PBS with 10% glycerol, 1.5% DDM, protease inhibitor cocktail and a mixture of polar lipids (Avanti polar lipids): 16:0–18:1 PC, 16:0–18:1 PE, 16:0–18:1 PG. Samples were centrifuged at $18,000 \times g$ for 10 min at 4°C to remove insoluble material. Soluble fractions were incubated with monoclonal anti-HA-agarose beads (Sigma) overnight at 4°C under gentle rotation. Anti-HA-agarose beads were washed five times using PBS with 10% glycerol, 0.05% DDM, protease inhibitor cocktail and polar lipids. Immunoabsorbed complexes were eluted under denaturing conditions using 200 mM glycine pH 2.5 and samples were subsequently neutralized with unbuffered 1 M Tris.

Transfection and generation of stable cell lines

S2R+ cells were transfected in 12-well plates using Effectene Transfection Reagent (Qiagen) according to the manufacturer's instructions. For immunofluorescence studies, cells were transiently

transfected and analyzed 24 h after transfection. For functional complementation studies, stable cells were obtained through selection with geneticin G418 (InvivoGen) at 1 mg/ml concentration for 30 days after transfection.

dsRNA synthesis and *in vitro* RNAi

Synthesis of dsRNA was performed using Ambion MEGAscript T7 Transcription Kit (ThermoFisher Scientific). dsRNAs for experiment and *mock* control treatment were synthesized using cDNA sequences from *D. melanogaster* CG7630 and human *IGFBP2*, respectively. The primers used for the amplification of T7 transcription template are listed in the table of primers (Table 1). For RNAi experiments, S2R+ cells were plated on 12-well plates and treated for 1 h with 5 µg synthetic dsRNA in Schneider's medium without serum. After treatment, serum was added and cells were harvested after 96 h.

Immunostaining and confocal microscopy

S2R+ cells were prepared for immunostaining and confocal microscopy as described previously (Benincá *et al*, 2021). The coverslips were mounted with Vectashield mounting medium (Vector Laboratories) and images were taken with a Zeiss LSM700 confocal microscope at 63× magnification. Antibodies used are listed Table 2.

Molecular modeling

Drosophila melanogaster cytochrome *c* oxidase model was built using the homology modeling protocol implemented in the MOE suite (Chemical Computing Group (CCG) Inc. (2020). *Molecular Operating Environment (MOE)*. Chemical Computing Group. <http://www.chemcomp.com>). A multiple template strategy was achieved by selecting bovine COX structure PDB-ID 2Y69 (Kaila *et al*, 2011, X-ray Crystallography, Resolution: 1.9 Å), the human COX PDB-ID 5Z62 (Zong *et al*, 2018, Cryo-EM, Resolution: 3.60 Å) and AlphaFold predicted structure (Uniprot: Q9VVG5, Jumper *et al*, 2021; Varadi *et al*, 2022) as templates. Human template was used to model NDUFA4/COXFA4 while the other 13 subunits were modeled on the bovine template. The mitochondrial targeting sequence at the N-terminal of CG7630 was identified with the MitoFates server (Fukasawa *et al*, 2015) and not further considered in the model generation. The CG7630 segment (23–51) was obtained from the AlphaFold database (Jumper *et al*, 2021; Varadi *et al*, 2022) as the corresponding template structure was not experimentally solved. The sequences were aligned with MOE except for CG7630 which alignment with COX7B was obtained from HHpred (Söding *et al*, 2005; Hildebrand *et al*, 2009). All the experimentally derived templates were prepared with the MOE structure preparation tool to add hydrogen atoms, fix missing atoms, and assign partial charges, and finally superposed. The homology model was obtained generating 10 different models using Amber12 Force Field (Maier *et al*, 2015) and selecting the best one according to the GB/VI score.

Statistical analysis

Statistical analysis was performed with GraphPad Prism Software, version 8.2.1. Statistical tests and significance are described in the figure captions.

Data availability

The structure of *D. melanogaster* COX obtained through molecular modeling is available in ModelArchive at <https://modelarchive.org/doi/10.5452/ma-ux9au>.

Expanded View for this article is available online.

Acknowledgements

We are grateful to Dr. Edward Owusu-Ansah (Columbia University, NY) for providing antibodies against *D. melanogaster* UQCR-C2 and SdhA. We are grateful to Prof. Rodolfo Costa (CNR institute of Neuroscience, Padova, Italy) for providing CG7630 RNAi line. MMS lab is very grateful to Chemical Computing Group for the scientific and technical partnership. Figure 1A was created with Biorender.com under a paid subscription. Our work is supported by: Telethon Foundation (GGP19007 to MZ and 20013 to CV); Fondation NRJ pour les Neurosciences—Institut de France Grant (to MZ); Associazione Luigi Comini Onlus (to MZ and CV), AFM—Telethon 23706 (to CV), Netherlands Organization for Health Research and Development (ZonMw) TOP grant 91217009 to SA and MH. Open Access Funding provided by Università degli Studi di Padova within the CRUI-CARE Agreement.

Author contributions

Michele Brischiaglio: Conceptualization; Data curation; Formal analysis; Validation; Investigation; Methodology; Writing—original draft; Writing—review and editing. **Alfredo Cabrera-Orefice:** Data curation; Formal analysis; Investigation; Methodology. **Mattia Sturlese:** Investigation; Methodology; Writing—original draft. **Dei M Elurbe:** Investigation. **Elena Frigo:** Investigation. **Erika Fernandez-Vizarra:** Supervision; Methodology. **Stefano Moro:** Supervision; Investigation; Methodology; Writing—original draft. **Martijn A Huynen:** Formal analysis; Funding acquisition; Investigation; Writing—original draft. **Susanne Arnold:** Data curation; Funding acquisition; Validation; Investigation; Writing—original draft. **Carlo Viscomi:** Supervision; Funding acquisition. **Massimo Zeviani:** Conceptualization; Supervision; Funding acquisition; Writing—original draft; Writing—review and editing.

In addition to the CRediT author contributions listed above, the contributions in detail are:

MB prepared samples for complexome profiling analysis and performed all the wet studies including molecular, cell biology, biochemical, and structural investigations, planning the experiments with MZ. ACO and SA performed the complexome profiling, analyzed and interpreted the data. MB, MS and SM performed the homology modelling study. EF contributed to RNAi validation, immunofluorescence, and phenotypical analyses. MB, DME and MH performed the phylogenetic analyses. CV and EFV provided technical advice and optimization. MZ conceived and supervised the project. MB and MZ wrote the manuscript. All authors discussed the results and contributed to the final version of the manuscript.

Disclosure and competing interests statement

The authors declare that they have no conflict of interest.

References

Acin-Perez R, Gatti DL, Bai Y, Manfredi G (2011) Protein phosphorylation and prevention of cytochrome oxidase inhibition by ATP: coupled mechanisms of energy metabolism regulation. *Cell Metab* 13: 712–719

- Balsa E, Marco R, Perales-Clemente E, Szklarczyk R, Calvo E, Landázuri MO, Enríquez JA (2012) NDUFA4 is a subunit of complex IV of the mammalian electron transport chain. *Cell Metab* 16: 378–386
- Benincá C, Zanette V, Brischiigliaro M, Johnson M, Reyes A, Do VDA, Robinson AJ, Degiorgi A, Yeates A, Telles BA et al (2021) Mutation in the MICOS subunit gene APOO (MIC26) associated with an X-linked recessive mitochondrial myopathy, lactic acidosis, cognitive impairment and autistic features. *J Med Genet* 58: 155–167
- Brandt T, Mourier A, Tain LS, Partridge L, Larsson NG, Kühlbrandt W (2017) Changes of mitochondrial ultrastructure and function during ageing in mice and *Drosophila*. *eLife* 6: e24662
- Bratton MR, Pressler MA, Hosler JP (1999) Suicide inactivation of cytochrome c oxidase: catalytic turnover in the absence of subunit III alters the active site. *Biochemistry* 38: 16236–16245
- Brischiigliaro M, Corrà S, Tregnago C, Fernandez-Vizarrá E, Zeviani M, Costa R, De Pittà C (2019) Knockdown of APOPT1/COA8 causes cytochrome c oxidase deficiency, neuromuscular impairment, and reduced resistance to oxidative stress in *Drosophila melanogaster*. *Front Physiol* 10: 1143
- Brischiigliaro M, Frigo E, Corrà S, De Pittà C, Szabò I, Zeviani M, Costa R (2021) Modelling of BCS1L-related human mitochondrial disease in *Drosophila melanogaster*. *J Mol Med* 99: 1471–1485
- Brischiigliaro M, Zeviani M (2021) Cytochrome c oxidase deficiency. *Biochim Biophys Acta Bioenerg* 1862: 148335
- Brischiigliaro M, Frigo E, Fernandez-Vizarrá E, Bernardi P, Viscomi C (2022) Measurement of mitochondrial respiratory chain enzymatic activities in *Drosophila melanogaster* samples. *STAR Protoc* 3: 101322
- Cabrera-Orefice A, Potter A, Evers F, Hevler JF, Guerrero-Castillo S (2022) Complexome profiling—exploring mitochondrial protein complexes in health and disease. *Front Cell Dev Biol* 9: 3707
- Carroll J, Fearnley IM, Skehel JM, Shannon RJ, Hirst J, Walker JE (2006) Bovine complex I is a complex of 45 different subunits. *J Biol Chem* 281: 32724–32727
- Clemens JC, Worby CA, Simonson-Leff N, Muda M, Maehama T, Hemmings BA, Dixon JE (2000) Use of double-stranded RNA interference in *Drosophila* cell lines to dissect signal transduction pathways. *Proc Natl Acad Sci USA* 97: 6499–6503
- Čunátová K, Reguera DP, Houštěk J, Mráček T, Pecina P (2020) Role of cytochrome c oxidase nuclear-encoded subunits in health and disease. *Physiol Res* 69: 947–965
- Esposti MD (2020) On the evolution of cytochrome oxidases consuming oxygen. *Biochim Biophys Acta Bioenerg* 1861: 148304
- van Esveld SL, Huynen MA (2018) Does mitochondrial DNA evolution in metazoa drive the origin of new mitochondrial proteins? *IUBMB Life* 70: 1240–1250
- Evers F, Cabrera-Orefice A, Elurbe DM, Kea-te Lindert M, Boltryk SD, Voss TS, Huynen MA, Brandt U, Kooij TWA (2021) Composition and stage dynamics of mitochondrial complexes in *Plasmodium falciparum*. *Nat Commun* 12: 3820
- Foriel S, Willems P, Smeitink J, Schenck A, Beyrath J (2015) Mitochondrial diseases: *Drosophila melanogaster* as a model to evaluate potential therapeutics. *Int J Biochem Cell Biol* 63: 60–65
- Foriel S, Herma Renkema G, Lasarzewski Y, Berkhout J, Rodenburg RJ, Smeitink JAM, Beyrath J, Schenck A (2019) A *Drosophila* mitochondrial complex I deficiency phenotype array. *Front Genet* 10: 245
- Fukasawa Y, Tsuji J, Fu SC, Tomii K, Horton P, Imai K (2015) MitoFates: improved prediction of mitochondrial targeting sequences and their cleavage sites. *Mol Cell Proteomics* 14: 1113–1126
- Fukuda R, Zhang H, Kim J-W, Shimoda L, Dang CV, Semenza G (2007) HIF-1 regulates cytochrome oxidase subunits to optimize efficiency of respiration in hypoxic cells. *Cell* 129: 111–122
- Garcia CJ, Khajeh J, Coulanges E, Chen EI, Owusu-Ansah E (2017) Regulation of mitochondrial complex I biogenesis in *Drosophila* flight muscles. *Cell Rep* 20: 264–278
- Giese H, Ackermann J, Heide H, Bleier L, Dröse S, Wittig I, Brandt U, Koch I (2015) NOVA: a software to analyze complexome profiling data. *Bioinformatics* 31: 440–441
- González M, Martín-Ruiz I, Jiménez S, Pirone L, Barrio R, Sutherland JD (2011) Generation of stable *Drosophila* cell lines using multicistronic vectors. *Sci Rep* 1: 75
- Guerrero-Castillo S, Baertling F, Kownatzki D, Wessels HJ, Arnold S, Brandt U, Nijtmans L (2017) The assembly pathway of mitochondrial respiratory chain complex I. *Cell Metab* 25: 128–139
- Hartley AM, Lukyanova N, Zhang Y, Cabrera-Orefice A, Arnold S, Meunier B, Pinotsis N, Maréchal A (2019) Structure of yeast cytochrome c oxidase in a supercomplex with cytochrome bc1. *Nat Struct Mol Biol* 26: 78–83
- Heide H, Bleier L, Steger M, Ackermann J, Dröse S, Schwamb B, Zörnig M, Reichert A, Koch I, Wittig I et al (2012) Complexome profiling identifies TMEM126B as a component of the mitochondrial complex I assembly complex. *Cell Metab* 16: 538–549
- Hevler JF, Chiozzi RZ, Cabrera-Orefice A, Brandt U, Arnold S, Heck AJR (2021) Molecular characterization of a complex of apoptosis-inducing factor 1 with cytochrome c oxidase of the mitochondrial respiratory chain. *Proc Natl Acad Sci USA* 118: e2106950118
- Hildebrand A, Remmert M, Biegert A, Söding J (2009) Fast and accurate automatic structure prediction with HHpred. *Proteins Struct Funct Bioinforma* 77: 128–132
- Hüttemann M, Lee I, Liu J, Grossman LI (2007) Transcription of mammalian cytochrome c oxidase subunit IV-2 is controlled by a novel conserved oxygen responsive element. *FEBS J* 274: 5737–5748
- Huynen MA, Duarte I, Szklarczyk R (2013) Loss, replacement and gain of proteins at the origin of the mitochondria. *Biochim Biophys Acta Bioenerg* 1827: 224–231
- Indrieri A, van Rahden V, Tiranti V, Morleo M, Iaconis D, Tammaro R, D'Amato I, Conte I, Maystadt I, Demuth S et al (2012) Mutations in COX7B cause microphthalmia with linear skin lesions, an unconventional mitochondrial disease. *Am J Hum Genet* 91: 942–949
- Jumper J, Evans R, Pritzel A, Green T, Figurnov M, Ronneberger O, Tunyasuvunakool K, Bates R, Žídek A, Potapenko A et al (2021) Highly accurate protein structure prediction with AlphaFold. *Nature* 596: 583–589
- Kahlhöfer F, Kmita K, Wittig I, Zwicker K, Zickermann V (2017) Accessory subunit NUYM (NDUFS4) is required for stability of the electron input module and activity of mitochondrial complex I. *Biochim Biophys Acta Bioenerg* 1858: 175–181
- Kaila VRI, Oksanen E, Goldman A, Bloch DA, Verkhovsky MI, Sundholm D, Wikström M (2011) A combined quantum chemical and crystallographic study on the oxidized binuclear center of cytochrome c oxidase. *Biochim Biophys Acta Bioenerg* 1807: 769–778
- Lieber T, Jeedigunta SP, Palozzi JM, Lehmann R, Hurd TR (2019) Mitochondrial fragmentation drives selective removal of deleterious mtDNA in the germline. *Nature* 570: 380–384
- Macleán AE, Bridges HR, Silva MF, Ding S, Ovcariškova J, Hirst J, Sheiner L (2021) Complexome profile of *Toxoplasma gondii* mitochondria identifies divergent subunits of respiratory chain complexes including new subunits of cytochrome bc1 complex. *PLoS Pathog* 17: e1009301
- Maier JA, Martinez C, Kasavajhala K, Wickstrom L, Hauser KE, Simmerling C (2015) ff14SB: improving the accuracy of protein side chain and backbone parameters from ff99SB. *J Chem Theory Comput* 11: 3696–3713

- Murari A, Rhooms SK, Goparaju NS, Villanueva M, Owusu-Ansah E (2020) An antibody toolbox to track complex I assembly defines AIF's mitochondrial function. *J Cell Biol* 219: e202001071
- Otera H, Ohsakaya S, Nagaura ZI, Ishihara N, Mihara K (2005) Export of mitochondrial AIF in response to proapoptotic stimuli depends on processing at the intermembrane space. *EMBO J* 24: 1375–1386
- Pajuelo Reguera D, Čunátová K, Vrbacký M, Pecinová A, Houštěk J, Mráček T, Pecina P (2020) Cytochrome c oxidase subunit 4 isoform exchange results in modulation of oxygen affinity. *Cells* 9: 443
- Páleníková P, Harbour ME, Prodi F, Minczuk M, Zeviani M, Ghelli A, Fernández-Vizcarra E (2021) Duplexing complexome profiling with SILAC to study human respiratory chain assembly defects. *Biochim Biophys Acta Bioenerg* 1862: 148395
- Pereira MM, Santana M, Teixeira M (2001) A novel scenario for the evolution of haem-copper oxygen reductases. *Biochim Biophys Acta Bioenerg* 1505: 185–208
- Peruzzo R, Corrà S, Costa R, Brischigliaro M, Varanita T, Biasutto L, Rampazzo C, Ghezzi D, Leanza L, Zoratti M et al (2021) Exploiting pyocyanin to treat mitochondrial disease due to respiratory complex III dysfunction. *Nat Commun* 12: 2103
- Pierron D, Wildman DE, Hüttemann M, Markondapatnaikuni GC, Aras S, Grossman LI (2012) Cytochrome c oxidase: evolution of control via nuclear subunit addition. *Biochim Biophys Acta Bioenerg* 1817: 590–597
- Pitceathly R, Rahman S, Wedatilake Y, Polke J, Cirak S, Foley A, Sailer A, Hurles M, Stalker J, Hargreaves I et al (2013) NDUFA4 mutations underlie dysfunction of a cytochrome c oxidase subunit linked to human neurological disease. *Cell Rep* 3: 1795–1805
- Pitceathly RDS, Taanman J-W (2018) NDUFA4 (renamed COXFA4) is a cytochrome-c oxidase subunit. *Trends Endocrinol Metab* 29: 452–454
- Potter SC, Luciani A, Eddy SR, Park Y, Lopez R, Finn RD (2018) HMMER web server: 2018 update. *Nucleic Acids Res* 46: W200–W204
- Scialò F, Sriram A, Stefanatos R, Spriggs RV, Loh SHY, Martins LM, Sanz A (2020) Mitochondrial complex I derived ROS regulate stress adaptation in *Drosophila melanogaster*. *Redox Biol* 32: 101450
- Senkler J, Senkler M, Eubel H, Hildebrandt T, Lengwenus C, Schertl P, Schwarzländer M, Wagner S, Wittig I, Braun HP (2017) The mitochondrial complexome of *Arabidopsis thaliana*. *Plant J* 89: 1079–1092
- Sharma V, Ala-Vanneluoma P, Vattulainen I, Wikström M, Róg T (2015) Role of subunit III and its lipids in the molecular mechanism of cytochrome c oxidase. *Biochim Biophys Acta Bioenerg* 1847: 690–697
- Söding J, Biegert A, Lupas AN (2005) The HHpred interactive server for protein homology detection and structure prediction. *Nucleic Acids Res* 33: W244–W248
- Szuplewski S, Terracol R (2001) The cyclope gene of *Drosophila* encodes a cytochrome c oxidase subunit Vic homolog. *Genetics* 158: 1629–1643
- Thompson K, Mai N, Oláhová M, Scialó F, Formosa LE, Stroud DA, Garrett M, Lax NZ, Robertson FM, Jou C et al (2018) OXA 1L mutations cause mitochondrial encephalopathy and a combined oxidative phosphorylation defect. *EMBO Mol Med* 10: e9060
- Varadi M, Anyango S, Deshpande M, Nair S, Natassia C, Yordanova G, Yuan D, Stroe O, Wood G, Laydon A et al (2022) AlphaFold Protein Structure Database: massively expanding the structural coverage of protein-sequence space with high-accuracy models. *Nucleic Acids Res* 50: D439–D444
- Wittig I, Malacarne PF (2021) Complexome profiling: assembly and remodeling of protein complexes. *Int J Mol Sci* 22: 7809
- Zhang J, Yang M, Wang W, Sun H, Xu Y, Ma L, Sun Y, Zhu C (2011) prag01, a novel deltamethrin-resistance-associated gene from *Culex pipiens pallens*. *Parasitol Res* 108: 417–423
- Zong S, Wu M, Gu J, Liu T, Guo R, Yang M (2018) Structure of the intact 14-subunit human cytochrome c oxidase. *Cell Res* 28: 1026–1034



License: This is an open access article under the terms of the Creative Commons Attribution-NonCommercial-NoDerivs License, which permits use and distribution in any medium, provided the original work is properly cited, the use is non-commercial and no modifications or adaptations are made.